

# Seed-Driven Stepwise Crystallization (SDSC) for Growing Rutile GeO<sub>2</sub> Films via MOCVD

Imteaz Rahaman<sup>1</sup>, Botong Li<sup>1</sup>, Bobby Duersch<sup>2</sup>, Hunter D. Ellis<sup>1</sup>, and Kai Fu<sup>1, a)</sup>

<sup>1</sup>*Department of Electrical and Computer Engineering, The University of Utah, Salt Lake City, UT 84112, USA*

<sup>2</sup>*Electron Microscopy and Surface Analysis Laboratory, The University of Utah, Salt Lake City, UT 84112, USA*

## Abstract

Germanium dioxide (r-GeO<sub>2</sub>) is an emerging new ultrawide bandgap (UWBG) semiconductor with significant potential for power electronics, thanks to its large-size substrate compatibility and ambipolar doping capability. However, phase segregation during metal-organic chemical vapor deposition (MOCVD) on substrates like r-TiO<sub>2</sub> has posed a significant barrier to achieving high-quality films. Conventional optimization of growth parameters has been found so far not very insufficient in film coverage and film quality. To address this, a seed-driven stepwise crystallization (SDSC) growth approach was employed in this study, featuring multiple sequential deposition steps on a pre-templated substrate enriched with r-GeO<sub>2</sub> seeds. The process began with an initial 180-minute deposition to establish r-GeO<sub>2</sub> nucleation seeds, followed by a sequence of shorter deposition steps (90, 60, 60, 60, 60, and 60 minutes). This stepwise growth strategy progressively increased the crystalline coverage to 57.4%, 77.49%, 79.73%, 93.27%, 99.17%, and ultimately 100%. Concurrently, the crystalline quality improved substantially, evidenced by a ~30% reduction in the Full Width at Half Maximum (FWHM) of X-ray diffraction rocking curves. These findings demonstrate the potential of the SDSC approach for overcoming phase segregation and achieving high-quality, large-area r-GeO<sub>2</sub> films.

---

a) Author to whom correspondence should be addressed. Electronic email: kai.fu@utah.edu

Ultrawide-bandgap (UWBG) semiconductors are becoming indispensable for next-generation power electronics and optoelectronic devices due to their exceptional electrical, thermal, and optical properties. Materials like  $\beta$ -Ga<sub>2</sub>O<sub>3</sub>, AlGa<sub>2</sub>N, and diamond exhibit high breakdown fields and superior power-handling capabilities, making them ideal for applications such as high-power transistors, UV detectors, and gas sensors.<sup>1-3</sup> However, despite their promise, each material faces intrinsic challenges:  $\beta$ -Ga<sub>2</sub>O<sub>3</sub> suffers from inefficient heat dissipation and a lack of p-type doping;<sup>4-</sup><sup>6</sup> AlGa<sub>2</sub>N experiences degraded acceptor activation and hole mobility with increasing Al content;<sup>7,8</sup> diamond production is hindered by limited wafer availability and doping difficulties.<sup>9,10</sup> Rutile GeO<sub>2</sub> (r-GeO<sub>2</sub>) has recently emerged as a promising UWBG semiconductor, exhibiting a bandgap of 4.44–4.68 eV<sup>11-13</sup>, electron mobility of 244 cm<sup>2</sup>/V·s  $\perp$ C and 377 cm<sup>2</sup>/V·s  $\parallel$ C<sup>14</sup>, and a Baliga figure of merit<sup>15</sup> of 27,000–35,000  $\times 10^6$  V<sup>2</sup>  $\Omega^{-1}$  cm<sup>-2</sup> surpassing that of  $\beta$ -Ga<sub>2</sub>O<sub>3</sub>. Its thermal conductivity, measured at 37 W/m·K (*a*-axis) and 58 W/m·K (*c*-axis), is nearly double that of  $\beta$ -Ga<sub>2</sub>O<sub>3</sub>.<sup>16</sup> Moreover, it is theoretically predicted to support ambipolar doping with promising hole mobility [27 cm<sup>2</sup>/Vs ( $\perp$  $\vec{C}$ )] and 29 ( $\parallel$  $\vec{C}$ )], paving the way for p-n junctions and flexible design of various power devices.<sup>12,14,17</sup> Furthermore, the rutile phase of GeO<sub>2</sub> is water-insoluble, unlike its  $\alpha$ -quartz counterpart.<sup>18</sup> It is also likely to demonstrate potential for bandgap tuning from 3.03 to 8.67 eV through alloying with other rutile oxides, such as r-SnO<sub>2</sub>, r-TiO<sub>2</sub>, and r-SiO<sub>2</sub>, similar to III-nitrides and (Al<sub>x</sub>Ga<sub>1-x</sub>)<sub>2</sub>O<sub>3</sub>.<sup>19-23</sup> Furthermore, the rutile TiO<sub>2</sub> has a small lattice mismatch with r-GeO<sub>2</sub>,<sup>24,25</sup> making it a practical substrate for r-GeO<sub>2</sub> epitaxy. However, achieving high-quality and wafer-scale r-GeO<sub>2</sub> films remains challenging due to the competition between other phases, such as  $\alpha$ -quartz and amorphous GeO<sub>2</sub>. Current epitaxial growth techniques, including molecular

beam epitaxy (MBE),<sup>26</sup> mist chemical vapor deposition (CVD),<sup>24</sup> metal-organic chemical vapor deposition (MOCVD)<sup>27,28</sup> and pulsed laser deposition (PLD),<sup>29-31</sup> have reported limited success in stabilizing the rutile phase. It is worth noting that Rahaman *et al.* demonstrated via MOCVD that while a 90-minute deposition enhanced film quality, a 180-minute deposition increased coverage of rutile GeO<sub>2</sub> but reduced quality.<sup>27</sup> Consequently, achieving full crystalline coverage while preserving good crystalline quality remains challenging during continuous deposition, regardless of whether the deposition time is short or long, due to phase segregation and defect formation.

In this work, a seed-driven stepwise crystallization (SDSC) approach has been implemented to overcome the epitaxy challenges by MOCVD. Through utilizing multiple deposition steps on the seeded template, the approach leverages nucleation seeds formed during the earlier stages of growth to enable full crystalline coverage of r-GeO<sub>2</sub> films on r-TiO<sub>2</sub> (001) substrates. The films were comprehensively characterized using techniques such as High-Resolution X-ray diffraction (HR-XRD), scanning electron microscopy (SEM), and reciprocal space mapping (RSM) to evaluate their crystal quality, morphology, and stress.

The GeO<sub>2</sub> films were grown using an Agilis MOCVD system manufactured by Agnitron Technology. The deposition process was conducted at a temperature of 925°C under a stable chamber pressure of 80 Torr. Tetraethyl germane (TEGe) and pure oxygen (O<sub>2</sub>) were utilized as precursors, with argon (Ar) functioning as both the carrier and shroud gas. The flow rates were 2000 SCCM for oxygen and 160 SCCM for the TEGe precursor while maintaining a susceptor rotation speed of 300 RPM for uniform deposition. The SDSC method was executed through incremental deposition steps, starting with an initial 180-minute step, followed by a 90-minute step, and subsequently five 60-minute intervals, all conducted under consistent growth conditions. Before introducing the substrates into the MOCVD chamber, the r-TiO<sub>2</sub> substrates underwent a

rigorous cleaning procedure, starting with a piranha solution ( $\text{H}_2\text{SO}_4:\text{H}_2\text{O}_2 = 3:1$ ) to remove organic contaminants, followed by sequential rinses with acetone, isopropanol, and deionized water. The structural characterization of the  $\text{GeO}_2$  thin films was performed using a Bruker D8 DISCOVER high-resolution XRD equipped with a  $\text{Cu K}\alpha_1$  source ( $\lambda = 1.5406 \text{ \AA}$ ), a triple-bounce channel-cut monochromator, and an Eiger R 250K detector. Surface morphology analysis was conducted using a Micron scale EDS Quanta 600F environmental SEM and a Bruker Dimension ICON AFM. ImageJ software was used to evaluate the coverage of the rutile  $\text{GeO}_2$  crystals. Table I provides a detailed summary of the sample IDs and the corresponding growth durations for each step.

Table I. Summary of sample IDs, corresponding growth steps, and their respective growth durations during the SDSC process.

<b>Sample ID</b>	<b>Sequence</b>	<b>Growth duration (min)</b>
T-22(0)	Step-1	180
T-22(1)	Step-2	90
T-22(2)	Step-3	60
T-22(3)	Step-4	60
T-22(4)	Step-5	60
T-22(5)	Step-6	60
T-22(6)	Step-7	60

Figure 1 illustrates the conventional nucleation mechanisms observed during the deposition of thin films, including  $r\text{-GeO}_2$  films on  $r\text{-TiO}_2$  substrate, and introduces the SDSC method for achieving uniform, high-quality films. The top section highlights two key growth phenomena: island growth and film coalescence. During the early stages of deposition, islands nucleate and grow independently on the substrate surface, forming localized crystalline regions.

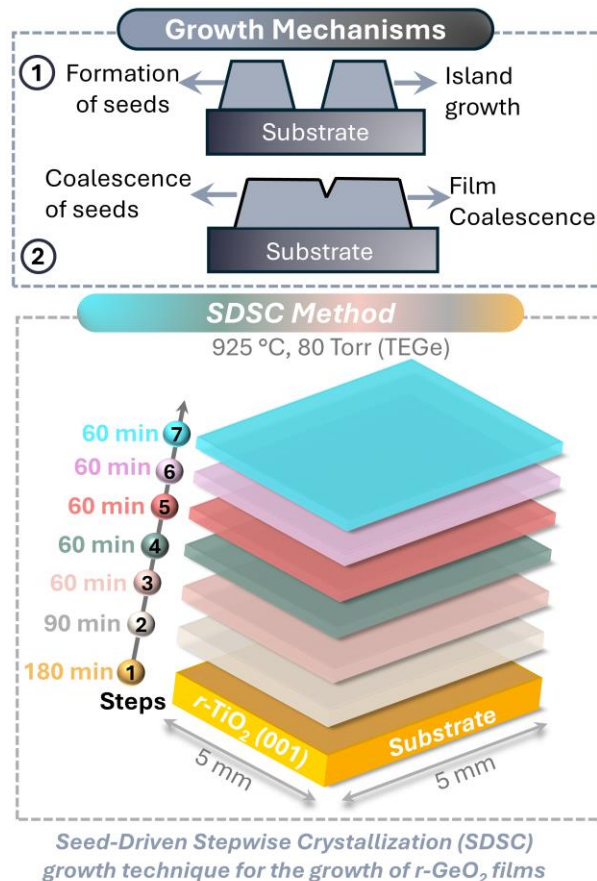


**FIG. 1.** Schematic representation of the SDSC growth process for r-GeO<sub>2</sub> films on r-TiO<sub>2</sub> (001) substrates. The top panel shows seed formation (island growth) and seed coalescence (film coalescence). The bottom panel illustrates the stepwise deposition process (Steps 1–7) to achieve uniform crystalline films on r-TiO<sub>2</sub> (001) substrates.

However, this process can lead to non-uniform film coverage with residual amorphous regions for GeO<sub>2</sub>.<sup>27</sup> To address this challenge, the SDSC method shown in the lower section employs a stepwise growth approach. The SDSC method employs incremental deposition steps to drive seed formation, expansion, and systematic coalescence of square-patterned regions. This step-by-step approach builds on the understanding of island growth and coalescence phenomena, ultimately aiming for a uniform, crystalline r-GeO<sub>2</sub> film with improved surface coverage of rutile phase GeO<sub>2</sub>.

Figure 2 illustrates the SEM images of the progressive evolution of r-GeO<sub>2</sub> coverage and morphology on the r-TiO<sub>2</sub> (001) substrate during the SDSC process. In the initial deposition stage (Step 1), isolated nucleation seeds of rutile r-GeO<sub>2</sub> (bright regions) are distinctly visible amidst significant uncovered substrate areas, representing the early stage of sparse island growth. As the process advances to the second deposition (Step 2), the nucleation density and island size noticeably increase and a distinct contrast emerges between the rutile GeO<sub>2</sub> phase (bright regions)<sup>32</sup> and the quartz/amorphous GeO<sub>2</sub> phase (dark regions)<sup>32</sup>.

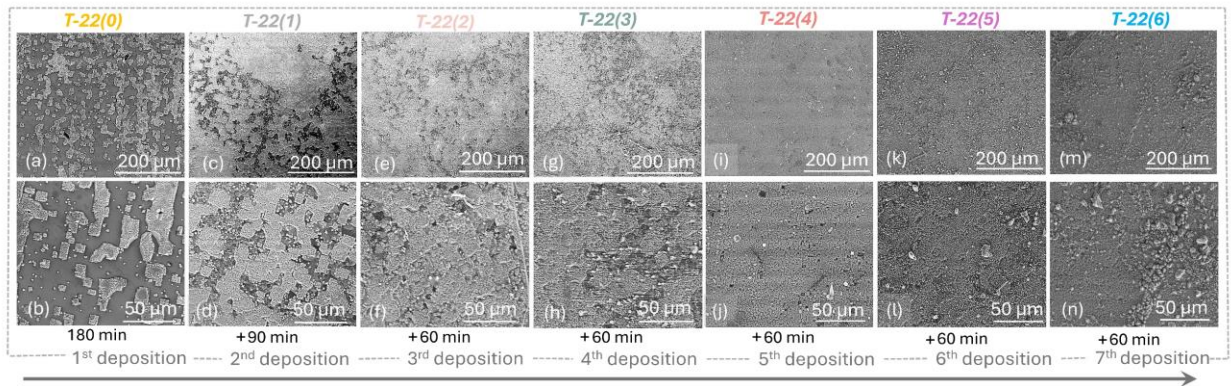


**FIG. 2.** SEM images showing the stepwise evolution of r-GeO<sub>2</sub> coverage on r-TiO<sub>2</sub> (001) substrate during the SDSC growth process. The progression highlights the increase in nucleation density and the dominance of rutile crystals through lateral growth and coalescence.

This multiple-phase coexistence arises from the thermodynamic competition among the rutile, quartz, cubic, and amorphous phases. During the intermediate stages (Steps 3 and 4), the rutile phase progressively dominates as nucleation sites expand laterally and vertically. This growth promotes the merging of adjacent crystalline domains, increasing coverage and leading to enhanced coalescence of rutile crystals. The stepwise growth strategy enhances adatom mobility and lateral diffusion, allowing nucleation seeds to coalesce into larger domains while minimizing competing phase formation.<sup>33–35</sup> Moreover, the coalescence of r-GeO<sub>2</sub> islands occurs to minimize the total surface energy of the system, as smaller islands tend to have higher energy due to their

larger surface-to-volume ratios. This thermodynamic driving force leads to the merging of nucleation sites.<sup>36,37</sup> The amorphous, cubic, and quartz phases are expected to be buried, as predicted by thermodynamic stability models.<sup>26,38</sup> In the later stages (Steps 5 through 7), the r-GeO<sub>2</sub> crystals become increasingly prominent as square-shaped structures, with the amorphous and quartz phases largely suppressed. After the 7<sup>th</sup> deposition, the surface achieves complete crystalline coverage, characterized by uniform and well-defined rutile crystals.

Figure 3 illustrates the corresponding evolution of surface morphology. Initially, the growth mode is characterized by isolated island nucleation (Step 1), where individual crystallites form.

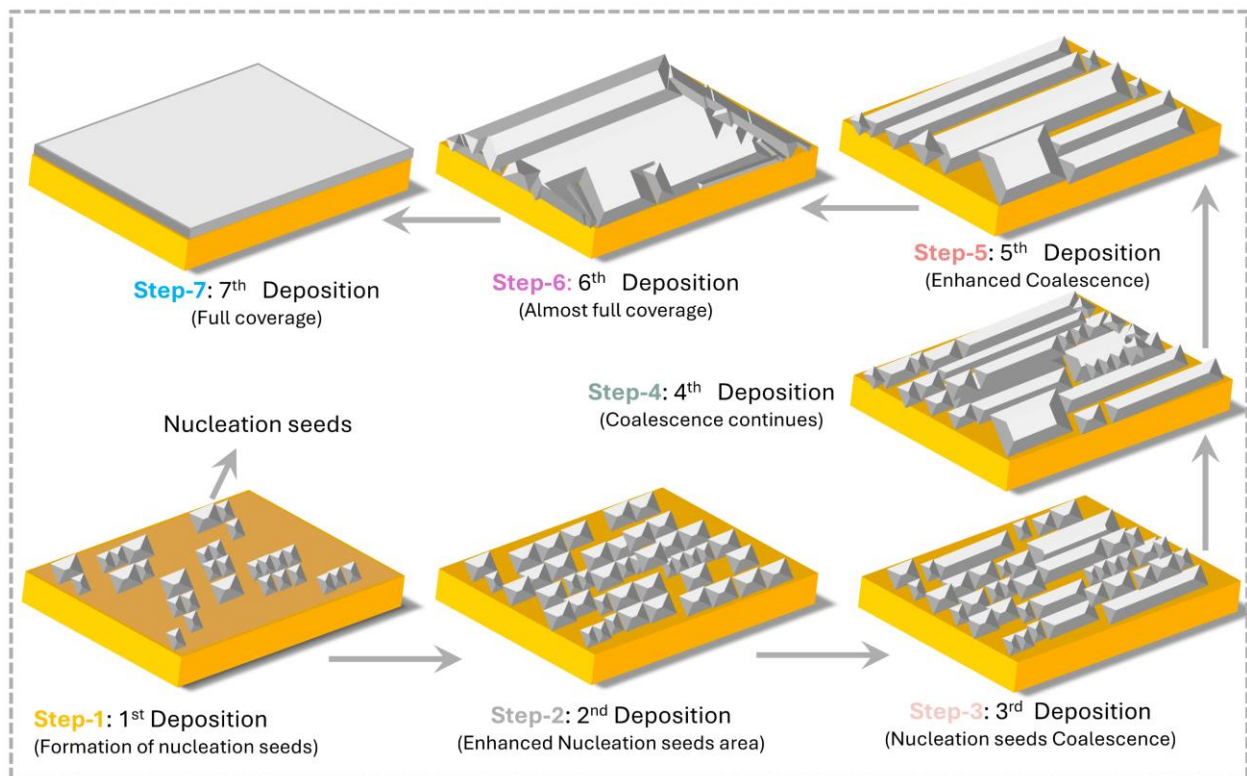


**FIG. 3.** Stepwise growth process of r-GeO<sub>2</sub> films using the SDSC method, showing nucleation seed formation (Step 1), enhanced nucleation area (Step 2), seed coalescence (Steps 3–5), and progression to full surface coverage (Steps 6–7).

Over subsequent steps, lateral growth and vertical expansion of these islands occur, driven by surface diffusion and adatom mobility, which enhance the merging of adjacent crystalline domains.<sup>34,39</sup> During the intermediate stages (Steps 3–5), coalescence dominates as the crystalline patterns coalesce into larger structures, minimizing surface energy and increasing coverage.<sup>33,36</sup> After Step 6 and Step 7, nearly full crystalline coverage is achieved, resulting in a fully continuous r-GeO<sub>2</sub> film.

Figure 4(a) presents the XRD  $2\theta$ - $\omega$  scan, where the prominent peak corresponding to the r-GeO<sub>2</sub> (002) plane, becomes increasingly intense with each deposition step, indicating a steady improvement in crystalline coverage. In contrast, peaks associated with other GeO<sub>2</sub> phases, such as cubic or hexagonal polymorphs, remain weak and diminish further in later steps, highlighting the selective stabilization and dominance of the rutile phase. This structural enhancement aligns well with the SEM observations, where the amorphous and quartz phases gradually become encapsulated beneath the growing rutile domains. Figure 4(b) shows the rocking curve ( $\omega$ -scan) measurements, revealing a progressive reduction in the FWHM ( $\Delta\omega$ ) from 0.37° after the first step to 0.259° after the final step. The consistent decrease in FWHM signifies a reduction in structural defects and improved crystalline uniformity, driven by the coalescence of rutile crystals during the stepwise growth process. Complementing this, Figure 4(c) plots the trends of FWHM (yellow) and rutile crystal coverage (gray), showing a clear correlation between decreasing FWHM and increasing coverage. Starting from ~45% in the initial step, the coverage steadily improves to ~100% in the final step.



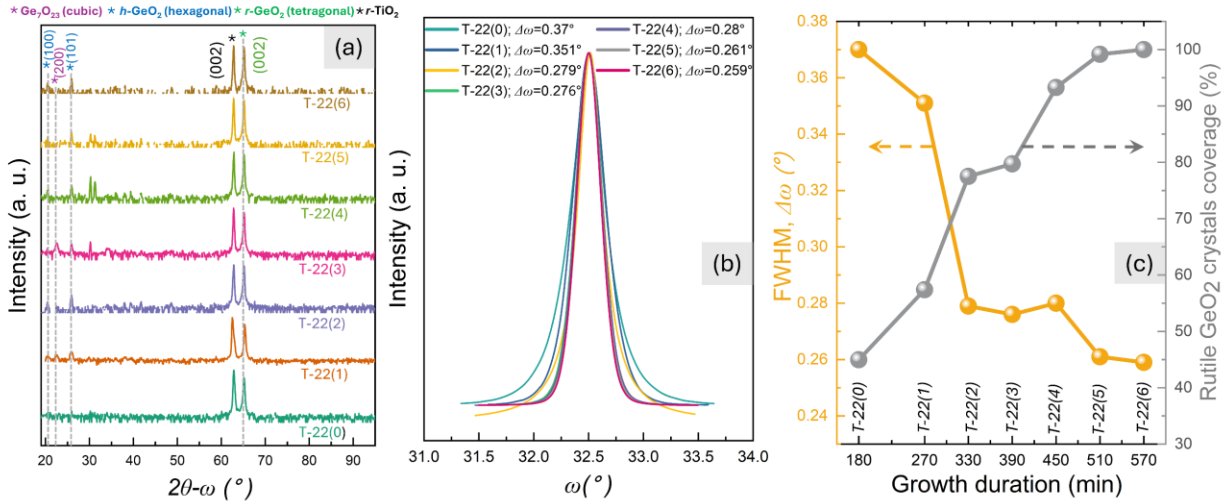


**FIG. 4.** Structural and morphological analysis of  $r\text{-GeO}_2$  films during the SDSC growth process. (a) XRD  $2\theta$ - $\omega$  scan showing the dominance of the rutile  $r\text{-GeO}_2$  (002) peak. (b) Rocking curve ( $\omega$ -scan) measurements demonstrating progressive improvement in crystalline quality with reduced FWHM ( $\Delta\omega$ ). (c) Trends of FWHM (yellow) and  $r\text{-GeO}_2$  crystal coverage (gray), highlighting simultaneous enhancement in crystalline quality and surface coverage through stepwise growth.

Figure 5 presents RSMs of symmetrical (002) and asymmetrical (022) reflections for the initial [T-22(0)] and final [T-22(6)] deposition steps of  $r\text{-GeO}_2$  films grown on the  $r\text{-TiO}_2$  (001) substrate. In the symmetrical RSMs [Figures 5(a) and 5(c)], the  $\text{GeO}_2$  (002) peak aligns closely with the  $\text{TiO}_2$  (002) substrate peak along the  $q_{\parallel}$ -direction across all steps, indicating minimal tilt of the  $c$ -axis and maintaining crystallographic orientation relative to the substrate. The asymmetrical RSMs displayed in Figures 5(b) and 5(d) show the (022) reflections of  $\text{GeO}_2$  and  $\text{TiO}_2$ . These reflections are characterized by  $K\alpha_1$  splitting and minimal broadening in the  $q_{\perp}$ -direction, which indicates the high structural quality of the films. Compared to T-22(0), the reflections in T-22(6) show less broadening in both the  $q_{\parallel}$  and  $q_{\perp}$ -directions, reflecting improved crystallographic alignment and reduced mosaicity, respectively,<sup>40</sup> thanks to the stepwise deposition process. However, the  $q_{\parallel}$  and  $q_{\perp}$  values of the film reflections deviate from those of the substrate reflections, as highlighted by

the triangular markers generated by Leptos 7.14 software for strain analysis. This shift indicates the presence of strain in films.

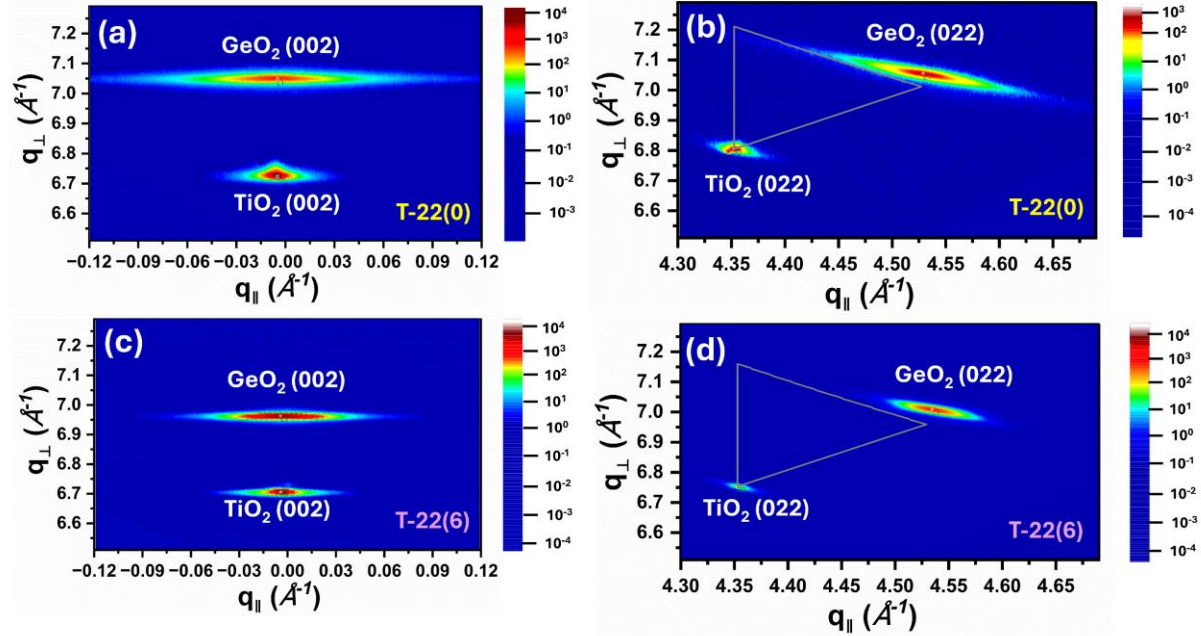


**FIG. 5.** Reciprocal space maps of r-GeO<sub>2</sub> films on r-TiO<sub>2</sub> substrates. Panels (a), and (b) show symmetric (002) reflections, while panels (b) and (d) display asymmetric (022) reflections for samples T-22(0) and T-22(6), respectively.

Quantitative analysis of the strain data from RSM plots reveals that the in-plane (lateral) strain increased from 0.757% for T-22(0) to 0.978% for T-22(6), while the out-of-plane (normal) strain also increased from 0.467% for T-22(0) to 0.603% for T-22(6). These results indicate that while crystalline quality improves, films experience a slight increase in strain as growth progresses. This behavior may arise due to the gradual coalescence of nucleation seeds into a continuous film, which introduces residual strain as the film grows.<sup>37</sup> The RMS roughness of the r-GeO<sub>2</sub> films is non-uniform across both the initial and final deposition steps. In the first step (T-22(0)), the roughness varies significantly, with an average RMS roughness of ~121.39 nm. After the final step (T-22(6)), the roughness remains non-uniform, with a measured average of 140.4 nm. While the

SDSC method successfully enhances crystalline growth, further optimization is needed to reduce the overall roughness.

In conclusion, a successful growth of high-coverage, crystalline rutile GeO<sub>2</sub> films on r-TiO<sub>2</sub> (001) substrates has been demonstrated using the SDSC method. Through sequential deposition steps, we achieved a significant improvement in both crystalline quality and surface coverage. The XRD and RSM analyses confirmed the dominance of the rutile phase while the rocking curve (FWHM) revealed a systematic reduction of ~30% in FWHM from 0.37° after the initial stage to 0.259° after the final step, indicating enhanced crystalline quality. SEM observations demonstrated the progressive evolution of crystalline square patterns, with coverage increasing from ~45% to 100%, validating the effectiveness of the SDSC method in promoting phase stability and film continuity. Although the SDSC method successfully achieved full rutile phase coverage and enhanced crystalline quality, addressing surface roughness remains a challenge requiring further improvement.

## **AUTHOR DECLARATIONS**

### **Conflict of Interest**

The authors have no conflicts to disclose.

### **Author Contributions**

Imteaz Rahaman: Data curation (lead); Formal analysis (lead); Investigation (lead); Methodology (lead), Writing-original draft (lead); Botong Li: Data curation(supporting); Writing – review & editing (supporting). Bobby Duersch: Data curation (supporting); Writing – review & editing (supporting), Formal analysis (supporting). Hunter D. Ellis: Writing – review & editing (supporting). Kai-Fu: Conceptualization (lead); Writing – review & editing (lead); Supervision (lead); Project administration (lead); Resources (lead).

## ACKNOWLEDGEMENT

The authors would like to express their sincere gratitude for the financial support received from the University of Utah's start-up fund and the PIVOT Energy Accelerator Grant U-7352FuEnergyAccelerator2023. Furthermore, they acknowledge the instrumental facilities provided by the University of Utah, which include the Utah Nanofab Cleanroom, the Material Characterization Meldrum, and the Nanofab Electron Microscopy and Surface Analysis Facilities.

## DATA AVAILABILITY

The data that supports the findings of this study are available from the corresponding authors upon reasonable request.

## REFERENCES

<sup>1</sup> B. Mallesham, S. Roy, S. Bose, A.N. Nair, S. Sreenivasan, V. Shutthanandan, and C.V. Ramana, “Crystal Chemistry, Band-Gap Red Shift, and Electrocatalytic Activity of Iron-Doped Gallium Oxide Ceramics,” *ACS Omega* **5**(1), 104–112 (2020).

<sup>2</sup> K. Fu, S. Luo, H. Fu, K. Hatch, S.R. Alugubelli, H. Liu, T. Li, M. Xu, Z. Mei, Z. He, J. Zhou, C. Chang, F.A. Ponce, R. Nemanich, and Y. Zhao, “GaN-Based Threshold Switching Behaviors at High Temperatures Enabled by Interface Engineering for Harsh Environment Memory Applications,” *IEEE Trans. Electron Devices*, 1–5 (2023).

<sup>3</sup> J.Y. Tsao, S. Chowdhury, M.A. Hollis, D. Jena, N.M. Johnson, K.A. Jones, R.J. Kaplar, S. Rajan, C.G. Van De Walle, E. Bellotti, C.L. Chua, R. Collazo, M.E. Coltrin, J.A. Cooper, K.R. Evans, S. Graham, T.A. Grotjohn, E.R. Heller, M. Higashiwaki, M.S. Islam, P.W. Juodawlkis, M.A. Khan, A.D. Koehler, J.H. Leach, U.K. Mishra, R.J. Nemanich, R.C.N. Pilawa-Podgurski, J.B. Shealy, Z.

Sitar, M.J. Tadjer, A.F. Witulski, M. Wraback, and J.A. Simmons, “Ultrawide-Bandgap Semiconductors: Research Opportunities and Challenges,” *Adv Elect Materials* **4**(1), 1600501 (2018).

<sup>4</sup> S.J. Pearton, J. Yang, P.H. Cary, F. Ren, J. Kim, M.J. Tadjer, and M.A. Mastro, “A review of Ga<sub>2</sub>O<sub>3</sub> materials, processing, and devices,” *Applied Physics Reviews* **5**(1), 011301 (2018).

<sup>5</sup> T. Kobayashi, T. Gake, Y. Kumagai, F. Oba, and Y. Matsushita, “Energetics and electronic structure of native point defects in  $\alpha$ -Ga<sub>2</sub>O<sub>3</sub>,” *Appl. Phys. Express* **12**(9), 091001 (2019).

<sup>6</sup> Y. Zhang, Q. Su, J. Zhu, S. Koirala, S.J. Koester, and X. Wang, “Thickness-dependent thermal conductivity of mechanically exfoliated  $\beta$ -Ga<sub>2</sub>O<sub>3</sub> thin films,” *Applied Physics Letters* **116**(20), 202101 (2020).

<sup>7</sup> K.B. Nam, M.L. Nakarmi, J. Li, J.Y. Lin, and H.X. Jiang, “Mg acceptor level in AlN probed by deep ultraviolet photoluminescence,” *Applied Physics Letters* **83**(5), 878–880 (2003).

<sup>8</sup> M.L. Nakarmi, K.H. Kim, M. Khizar, Z.Y. Fan, J.Y. Lin, and H.X. Jiang, “Electrical and optical properties of Mg-doped Al<sub>0.7</sub>Ga<sub>0.3</sub>N alloys,” *Applied Physics Letters* **86**(9), 092108 (2005).

<sup>9</sup> M.W. Geis, T.C. Wade, C.H. Wuorio, T.H. Fedynyshyn, B. Duncan, M.E. Plaut, J.O. Varghese, S.M. Warnock, S.A. Vitale, and M.A. Hollis, “Progress Toward Diamond Power Field-Effect Transistors,” *Physica Status Solidi (a)* **215**(22), 1800681 (2018).

<sup>10</sup> I. Rahaman, M. Sultana, R. Medina, I.H. Emu, and A. Haque, “Optimization of Electrostatic Seeding Technique for Wafer-Scale Diamond Fabrication on B-Ga<sub>2</sub>O<sub>3</sub>,” (2024).

<sup>11</sup> M. Stapelbroek, and B.D. Evans, “Exciton structure in the u.v.-absorption edge of tetragonal GeO<sub>2</sub>,” *Solid State Communications* **25**(11), 959–962 (1978).

<sup>12</sup> S. Chae, J. Lee, K.A. Mengle, J.T. Heron, and E. Kioupakis, “Rutile GeO<sub>2</sub>: An ultrawide-band-gap semiconductor with ambipolar doping,” *Applied Physics Letters* **114**(10), 102104 (2019).

- <sup>13</sup> K.A. Mengle, S. Chae, and E. Kioupakis, “Quasiparticle band structure and optical properties of rutile GeO<sub>2</sub>, an ultra-wide-band-gap semiconductor,” *Journal of Applied Physics* **126**(8), 085703 (2019).
- <sup>14</sup> K. Bushick, K.A. Mengle, S. Chae, and E. Kioupakis, “Electron and hole mobility of rutile GeO<sub>2</sub> from first principles: An ultrawide-bandgap semiconductor for power electronics,” *Applied Physics Letters* **117**(18), 182104 (2020).
- <sup>15</sup> S. Chae, K. Mengle, K. Bushick, J. Lee, N. Sanders, Z. Deng, Z. Mi, P.F.P. Poudeu, H. Paik, J.T. Heron, and E. Kioupakis, “Toward the predictive discovery of ambipolarly dopable ultra-wide-band-gap semiconductors: The case of rutile GeO<sub>2</sub>,” *Applied Physics Letters* **118**(26), 260501 (2021).
- <sup>16</sup> S. Chae, K.A. Mengle, R. Lu, A. Olvera, N. Sanders, J. Lee, P.F.P. Poudeu, J.T. Heron, and E. Kioupakis, “Thermal conductivity of rutile germanium dioxide,” *Applied Physics Letters* **117**(10), 102106 (2020).
- <sup>17</sup> C.A. Niedermeier, K. Ide, T. Katase, H. Hosono, and T. Kamiya, “Shallow Valence Band of Rutile GeO<sub>2</sub> and P-type Doping,” *J. Phys. Chem. C* **124**(47), 25721–25728 (2020).
- <sup>18</sup> K. Shimazoe, T. Ogawa, and H. Nishinaka, “Growth of water-insoluble rutile GeO<sub>2</sub> thin films on (001) TiO<sub>2</sub> substrates with graded Ge<sub>x</sub> Sn<sub>1-x</sub> O<sub>2</sub> buffer layers,” *Appl. Phys. Express* **17**(10), 105501 (2024).
- <sup>19</sup> H. Takane, Y. Ota, T. Wakamatsu, T. Araki, K. Tanaka, and K. Kaneko, “Band-gap engineering of rutile-structured SnO<sub>2</sub> – GeO<sub>2</sub> – SiO<sub>2</sub> alloy system,” *Phys. Rev. Materials* **6**(8), 084604 (2022).

- <sup>20</sup> Y. Nagashima, M. Fukumoto, M. Tsuchii, Y. Sugisawa, D. Sekiba, T. Hasegawa, and Y. Hirose, “Deep Ultraviolet Transparent Electrode: Ta-Doped Rutile  $\text{Sn}_{1-x}\text{Ge}_x\text{O}_2$ ,” *Chem. Mater.* **34**(24), 10842–10848 (2022).
- <sup>21</sup> J. Chen, Z. Zhang, Y. Guo, and J. Robertson, “Revisiting the electronic and optical properties of  $\text{SiO}_2$  polymorphs by hybrid functional calculations,” *Journal of Applied Physics* **133**(4), 044101 (2023).
- <sup>22</sup> S. Fujita, and K. Kaneko, “Epitaxial growth of corundum-structured wide band gap III-oxide semiconductor thin films,” *Journal of Crystal Growth* **401**, 588–592 (2014).
- <sup>23</sup> B. Amin, I. Ahmad, M. Maqbool, S. Goumri-Said, and R. Ahmad, “*Ab initio* study of the bandgap engineering of  $\text{Al}_{1-x}\text{Ga}_x\text{N}$  for optoelectronic applications,” *Journal of Applied Physics* **109**(2), 023109 (2011).
- <sup>24</sup> H. Takane, and K. Kaneko, “Establishment of a growth route of crystallized rutile  $\text{GeO}_2$  thin film ( $\geq 1 \mu\text{m/h}$ ) and its structural properties,” *Applied Physics Letters* **119**(6), 062104 (2021).
- <sup>25</sup> S. Chae, L.A. Pressley, H. Paik, J. Gim, D. Werder, B.H. Goodge, L.F. Kourkoutis, R. Hovden, T.M. McQueen, E. Kioupakis, and J.T. Heron, “Germanium dioxide: A new rutile substrate for epitaxial film growth,” *Journal of Vacuum Science & Technology A* **40**(5), 050401 (2022).
- <sup>26</sup> S. Chae, H. Paik, N.M. Vu, E. Kioupakis, and J.T. Heron, “Epitaxial stabilization of rutile germanium oxide thin film by molecular beam epitaxy,” *Applied Physics Letters* **117**(7), 072105 (2020).
- <sup>27</sup> I. Rahaman, B.G. Duersch, H.D. Ellis, M.A. Scarpulla, and K. Fu, “Epitaxial growth of rutile  $\text{GeO}_2$  via MOCVD,” *Applied Physics Letters* **125**(10), 102103 (2024).
- <sup>28</sup> I. Rahaman, H.D. Ellis, K. Anderson, M.A. Scarpulla, and K. Fu, “Growth of  $\text{GeO}_2$  on *R*-Plane and *C*-Plane Sapphires by MOCVD,” *ACS Appl. Eng. Mater.* **2**(6), 1724–1736 (2024).

- <sup>29</sup> G. Deng, K. Saito, T. Tanaka, M. Arita, and Q. Guo, “Pulsed laser deposition growth of ultra-wide bandgap GeO<sub>2</sub> film and its optical properties,” *Applied Physics Letters* **119**(18), 182101 (2021).
- <sup>30</sup> G. Deng, Y. Huang, Z. Chen, K. Saito, T. Tanaka, M. Arita, and Q. Guo, “Heteroepitaxy of (1 0 0)-oriented rutile GeO<sub>2</sub> film on c-plane sapphire by pulsed laser deposition,” *Materials Letters* **326**, 132945 (2022).
- <sup>31</sup> G. Deng, Y. Huang, Z. Chen, K. Saito, T. Tanaka, M. Arita, and Q. Guo, “Temperature-dependent photoluminescence of r-GeO<sub>2</sub> film deposited on r-plane sapphire by synchrotron radiation excitation,” *Journal of Luminescence* **267**, 120353 (2024).
- <sup>32</sup> I. Rahaman, B. Li, H.D. Ellis, B.R. Van Devener, R.C. Polson, and K. Fu, “A TEM Study of MOCVD-Grown Rutile GeO<sub>2</sub> Films,” (2024).
- <sup>33</sup> A. Pimpinelli, and J. Villain, *Physics of Crystal Growth*, 1st ed. (Cambridge University Press, 1998).
- <sup>34</sup> Z. Zhang, and M.G. Lagally, “Atomistic Processes in the Early Stages of Thin-Film Growth,” *Science* **276**(5311), 377–383 (1997).
- <sup>35</sup> B.W. Sheldon, K.H.A. Lau, and A. Rajamani, “Intrinsic stress, island coalescence, and surface roughness during the growth of polycrystalline films,” *Journal of Applied Physics* **90**(10), 5097–5103 (2001).
- <sup>36</sup> J.A. Thornton, “Influence of apparatus geometry and deposition conditions on the structure and topography of thick sputtered coatings,” *Journal of Vacuum Science and Technology* **11**(4), 666–670 (1974).
- <sup>37</sup> S.C. Seel, J.J. Hoyt, E.B. Webb, and J.A. Zimmerman, “Modeling metallic island coalescence stress via adhesive contact between surfaces,” *Phys. Rev. B* **73**(24), 245402 (2006).



<sup>38</sup> A.A. Bolzan, C. Fong, B.J. Kennedy, and C.J. Howard, “Structural Studies of Rutile-Type Metal Dioxides,” *Acta Crystallogr B Struct Sci* **53**(3), 373–380 (1997).

<sup>39</sup> J.A. Venables, G.D.T. Spiller, and M. Hanbucken, “Nucleation and growth of thin films,” *Rep. Prog. Phys.* **47**(4), 399–459 (1984).

<sup>40</sup> M. Kneiß, A. Hassa, D. Splith, C. Sturm, H. Von Wenckstern, T. Schultz, N. Koch, M. Lorenz, and M. Grundmann, “Tin-assisted heteroepitaxial PLD-growth of  $\kappa$ -Ga<sub>2</sub>O<sub>3</sub> thin films with high crystalline quality,” *APL Materials* **7**(2), 022516 (2019).